Journal of Materials Chemistry A

PAPER

View Article Online
View Journal | View Issue

Cite this: J. Mater. Chem. A, 2015, 3, 6835

Significant piezoelectric and energy harvesting enhancement of poly(vinylidene fluoride)/polypeptide fiber composites prepared through near-field electrospinning†

Cheng-Tang Pan,[a] Chung-Kun Yen,[a] Hui-Chun Wu,[a] Liwei Lin,[b] Yi-Syuan Lu,[c] Jacob Chih-Ching Huang[c] and Shiao-Wei Kuo*[c]

Received 7th January 2015
Accepted 10th February 2015

DOI: 10.1039/c5ta00147a

www.rsc.org/MaterialsA

In this study we applied near-field electrospinning (NFES) to prepare ordered poly(vinylidene fluoride) (PVDF)/poly(γ-methyl L-glutamate) (PMLG) composite fibers displaying enhanced piezoelectricity. Using Fourier transform infrared (FTIR) spectroscopy and differential scanning calorimetry (DSC), we analyzed the miscibility, specific interactions, and secondary structures of the PVDF/PMLG composites. The NFES process improved the piezoelectric properties of the PMLG/PVDF composites, resulting in better orientation of their dipoles, a high ultimate stress (27.47 MPa), and a high Young's modulus (2.77 GPa), as determined through micro-tensile testing. After patterning PVDF/PMLG piezoelectric composite fibers onto a poly(ethylene terephthalate)-based structure with parallel electrodes, we obtained a flexible PVDF/PMLG energy harvester that could capture ambient energy with a maximum peak voltage of 0.08 V, a power of 637.81 pW, and the energy conversion efficiency is 3.3%. The electro-mechanical energy conversion efficiency of this PVDF/PMLG energy harvester was up to three times higher than those of pristine individual PVDF and PMLG energy harvesters. Such PMLG/PVDF piezoelectric composite fibers exhibiting good piezoelectricity and good mechanical properties might have applicability in several fields, including biomedical engineering, green energy, wearable sensors, and energy harvesting.

Introduction

Although batteries are common as embedded power supplies in conventional wireless devices, they have only a finite amount of energy, a limited life, and result in potentially hazardous chemical pollution.[1–4] Accordingly, much research effort has been exerted to improve the size, weight, power density, economical efficiency, and environmental friendliness of power sources. Recent advances in electro-mechanical technology have led to rapid growth in demand for means of powering sensors. Because vibration is ubiquitous in real environments, the conversion of ambient mechanical vibration to electrical energy appears to be one of the most potentially useful methods for powering wireless sensors without the generation of the hazardous byproducts associated with other forms of power generation.[5,6] In addition, the power source would not need to be replaced or occasionally replenished with fuel, unlike batteries. Vibration-based energy harvesters incorporating piezoelectric materials that harvest environmentally random energy (*e.g.*, irregular vibrations, light airflow, human activity) have attracted considerable attention. Vibration energy harvesters or energy scavengers recover mechanical energy from their surrounding environments and convert it into useable electricity to drive microwatt-scale powered electronics.

Piezoelectric materials are powering transducers possessing crystalline structures, which provide the materials with the ability to transform mechanical strain energy into electrical charge. This captured energy can then be used to prolong the life of the power supply.[7] Near-field electrospinning (NFES)[8,9] is a method that can be used to fabricate controllable fibers having diameters ranging from a few micrometers down to a few nanometers.[10] This process can be applied to synthetic and natural polymers, polymer alloys, polymer composites, as well as electrospun fibers of the polypeptide poly(γ-benzyl-L-glutamate) metals and ceramics.[11] These electrospun fibers are particularly attractive because of their high porosity, small diameter, excellent pore interconnectivity, and high surface-to-volume ratio.[12]

[a]Department of Mechanical and Electro-Mechanical Engineering, National Sun Yat-Sen University, Kaohsiung 80424, Taiwan

[b]Department of Mechanical Engineering and Berkeley Sensor and Actuator Center, University of California, Berkeley, California 94720, USA

[c]Department of Materials and Optoelectronic Science, Center for Functional Polymers and Supramolecular Materials, National Sun Yat-Sen University, Kaohsiung 80424, Taiwan. E-mail: kuosw@faculty.nsysu.edu.tw

† Electronic supplementary information (ESI) available. See DOI: 10.1039/c5ta00147a

Most previous studies of piezoelectric polymer materials have used poly(vinylidene difluoride) (PVDF) as the substrate. For example, Andrew and Clark reported elevated levels of the β-crystalline phase (all-*trans* conformation) in electrospun PVDF fibers, due to both stretching of the polymer chains and the electric field between the needle tip and the collector.[13] In contrast, PVDF possesses a random coil conformation in solution, from which it requires a higher energy to be poled by the electric field. As a result, the use of rod-like polymers is quite important when preparing new piezoelectric polymeric materials. For example, Farrar *et al.* prepared electrospun fibers of the polypeptide poly(γ-benzyl-L-glutamate) (PBLG) and Ren *et al.* combined electrospinning with a hot press method to prepare poled PBLG films.[14,15] In a previous study, we examined the electrical energy conversion and mechanical characteristics of piezoelectric fibers of synthetic PBLG prepared through cylindrical near-field electrospinning (CNFES); PBLG piezoelectric fibers patterned directly on a cicada wing, with an interdigitated electrode for energy harvesting and a vibrational frequency of approximately 30 Hz, produced voltages up to 14.25 mV.[16]

In addition to using pure homopolymers to prepare the fiber structures, composite fibers offer many distinct attractions, including enhanced mechanical, thermal, and electrical properties.[17] In addition, the multiphase construction of composite fibers yields more-robust actuators.[18] Breuer and Sundararaj performed a study of such polymer composites with emphasis placed on their applications, processing methods, and physical properties.[19] Similarly, Huang *et al.* focused the scope of their study of the electrospinning of polymer composite fibers on their applications, processing, and characterization methods.[12]

In this present study we found that, when using the NFES process, the orientation of poly(γ-methyl L-glutamate) (PMLG) can be altered through blending with the host polymer PVDF. During the electrospinning process, the α-helix of the polypeptide can be rearranged to enhance the piezoelectric properties[16,20] and the non-polar α-phase of the PVDF solution also can be transformed into the polar β-phase,[21] which is responsible for the piezoelectric properties of the PVDF polymer. We have used differential scanning calorimetry (DSC), Fourier transform infrared (FTIR) spectroscopy, and wide-angle X-ray diffraction (WAXD) to analyze the hydrogen-bonding interactions and secondary structures of these PMLG/PVDF composite fibers designed for power generation.[22–25] To enhance the power output, in this study we used {3–3} piezoelectric mode to investigate the PMLG/PVDF fibers in vibration tests, because the output voltage of the {3–3} mode was twice that of the {3–1} mode.

Experimental section

Materials

γ-Methyl L-glutamate *N*-carboxyanhydride (MLG NCA) monomer and PMLG (M_n = 6500) were prepared according to literature procedures.[24] PVDF powder (M_n = 534 000), acetone, and dimethyl sulfoxide (DMSO) were purchased from Sigma-Aldrich (USA). Blends of PMLG/PVDF at various blend compositions were prepared through solution-casting. A DMF solution of the polymer mixture was stirred for 6–8 h and then the solvent was evaporated slowly at 100 °C for 1 day. The film of the blend was then dried at 120 °C for 2 days to ensure total removal of the residual solvent.

CNFES process

In this study, we focus on the NFES process to fabricate piezoelectric PMLG/PVDF composite fibers. A cylindrical glass tube was used to collect the electrospun fibers during the NFES process. Comparing NFES with conventional far field electrospinning (FFES), the NFES process shows superior mechanical stretching for possible alignment of dipoles along the longitudinal direction of the fibers. Therefore, the piezoelectricity of fibers fabricated by NFES is better than that by FFES. The

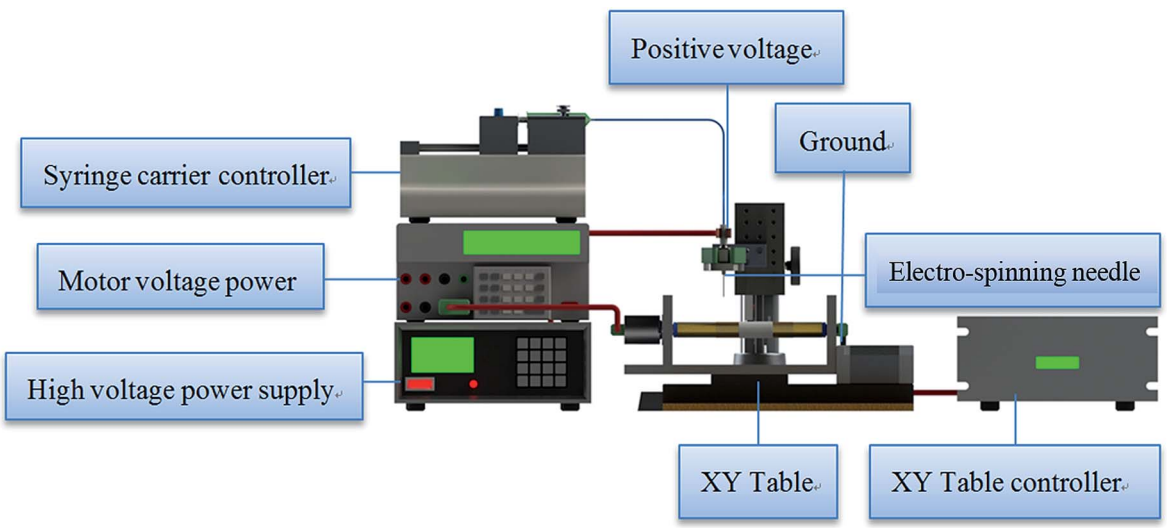

Scheme 1 Schematic representation of the NFES process on a glass tube.

experimental setup of the NFES system (Scheme 1) included a needle clamping apparatus, an infusion pump, a high-voltage power supply, a glass tube collector mounted on a motor, and an X–Y motion stage (controlled by an X–Y stage controller *via* a computer). A high voltage of 10–16 kV was applied to create a high electric field (1×10^7 to 1.6×10^7 V m^{-1}) between the needle and the collector (the gap between them was 1–2 mm).

Inducing electric potential from the mechanical strain rate

The piezoelectric harvester was developed to convert mechanical vibration to electrical power. 5 mm long piezoelectric fibers (*ca.* 120 fibers; stacked area: 5 mm × 5 mm) were placed on a piece of flexible poly(ethylene terephthalate) (PET) with both ends bonded tightly to parallel copper electrodes to achieve a large displacement. Fig. S1(a) and (b)† provide schematic representations of the PET vibrational structure and the vibration measurement system. The harvester was characterized under repeated external strains, using a DC motor to control the deformation magnitude. The mechanical strains distributed along the fibers were then converted to alternating voltage and current through the piezoelectric {3–3} mode. Fig. S2† displays a schematic representation of the measurement system. A rod connected to a rotary motor was used to produce a low-frequency vibration at the free end of the cantilever plate, producing axial strain upon the piezoelectric fibers. An infrared tachometer was used to measure the rotational speed of the motor and convert it into frequency. A power supply was used to drive the motor and control the angular speed. The induced electric potential and current signals from the harvester were measured using voltage and current measurement meters, respectively. A strain gauge was used to measure the strain of the electrospun fibers at the free end of the cantilever plate.

Results and discussion

Miscibility, interaction and crystalline structures of PMLG/PVDF blends

Thermal characterization of polymer blends can be used to determine the miscibility of polymer blends.[26] Fig. 1 presents the second heating runs of our DSC analyses of PMLG blends with PVDF at various compositions. For pure PMLG, it shows only the glass transition temperature at *ca.* 48 °C as shown in Fig. 1(a) and we observed clear melting point and crystallization

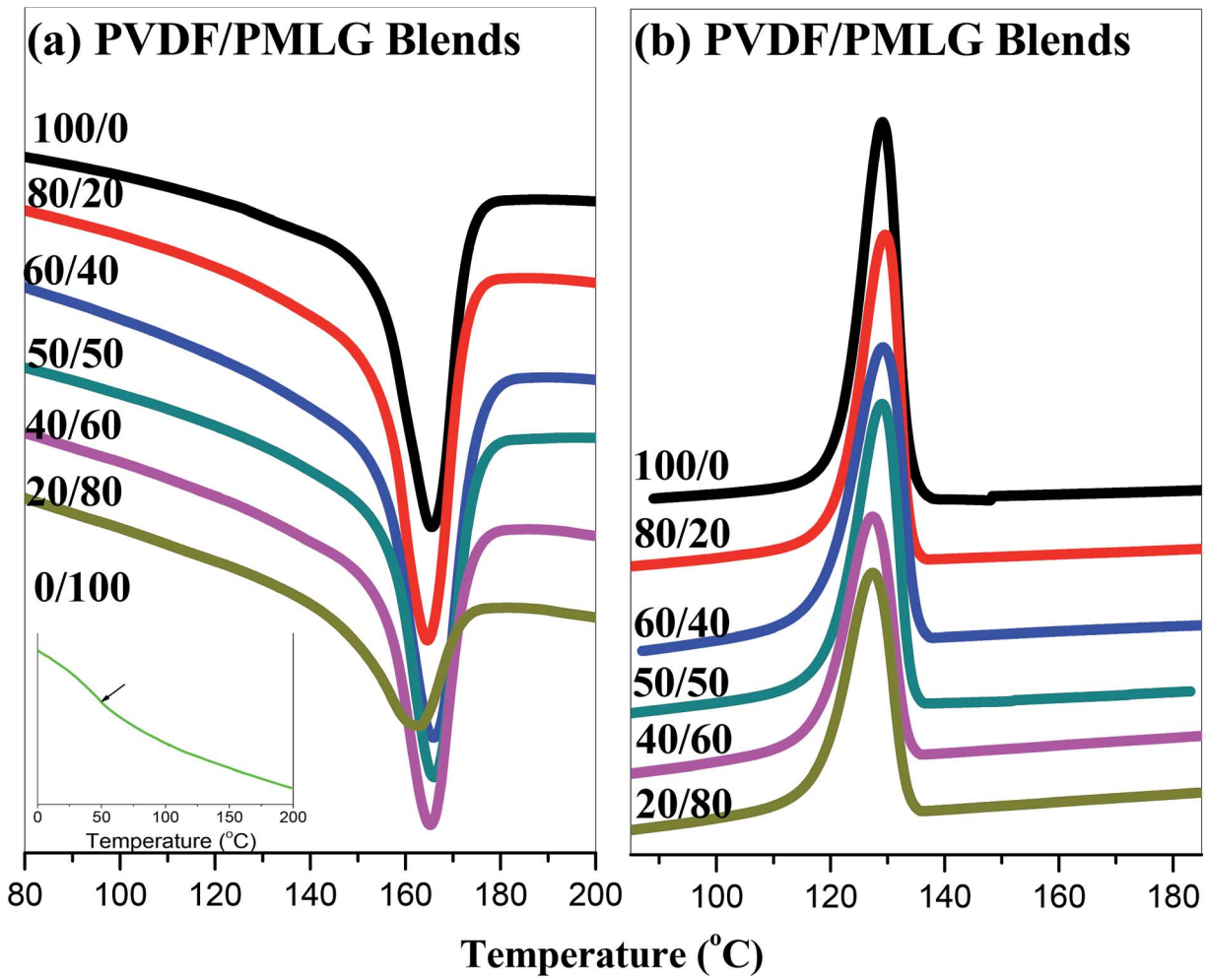

Fig. 1 DSC thermograms of PVDF/PMLG blends: (a) heating and (b) cooling scans.

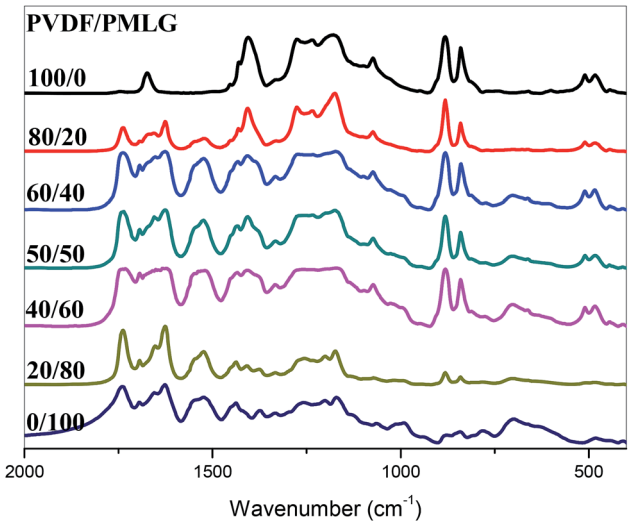

Fig. 2 FTIR spectra, measured at room temperature, of solution-cast samples of PVDF/PMLG blends.

depression, consistent with thermodynamic mixing of a crystalline polymer with an amorphous polymer, indicating that PMLG and PVDF were miscible at the molecular level.[27] The melting temperature decreased from 166.1 °C for pure PVDF to 162.5 °C for its blend with 80 wt% of PMLG. In addition, the PMLG/PVDF blends retained their crystalline structure, even at high PMLG contents.

Fig. 2 displays FTIR spectra (in the range 2000–400 cm^{-1}) of PMLG/PVDF blends, recorded at room temperature. Analyzing the spectrum of pure PMLG using the second derivative technique,[22] we observed four major peaks between 1800 and 1600 cm^{-1}, representing the free C=O groups (1743 cm^{-1}) and the secondary structures of the amide I groups in β-turn sheets (1696 cm^{-1})[22] and the α-helical (1656 cm^{-1})[24] and β-sheet (1624 cm^{-1})[24] conformations. For pure PVDF, the signals for the β-phase were located at 470, 511, 840, and 1274 cm^{-1}, indicating that our sample of PVDF used in this study existed in the β-phase (all-*trans* conformation).[27–29] The β-phase did not disappear completely when blending with PMLG at relatively low contents; its signals disappeared only when the PMLG content in the blend was at least 80 wt%. In addition, we assign the signal at 1743 cm^{-1} to the absorption of the free C=O groups of PMLG. This band shifted to a lower frequency, from 1743 to 1737 cm^{-1}, upon blending [Fig. 3(a)], consistent with intermolecular interactions occurring between the C=O groups of PMLG and the CH_2 groups of PVDF,[30] as depicted in Scheme 2. Furthermore, we fitted a series of Gaussian distributions to quantify the fractions of secondary structures of each of the peaks located between 1800 and 1600 cm^{-1}. Fig. 3(b) summarizes the curve fitting data for the amide I groups of the β-sheet and α-helical structures; we observe that the fraction of α-helical conformations of PMLG increased continuously upon increasing the PVDF content.

Next, we used WAXD to identify the changes occurring in the secondary structures and crystalline structures of the PMLG/PVDF blends (Fig. 4). For pure PMLG, the diffraction pattern revealed the presence of both α-helical and β-sheet secondary structures. We observed a diffraction peak at a value of q of 0.56, associated with α-helical secondary structures, corresponding to two-dimensional (2D) hexagonal packing of cylinders composed of 18/5 α-helices having a cylinder distance of 1.12 nm.[24,31] A weak peak at a value of q of 0.38 reflected the distance (d = 1.76 nm) between the backbones in the antiparallel β-pleated sheet structure; a reflection at a value of q of 1.34 (d = 0.468 nm) represented the intermolecular distance between adjacent peptide chains within one lamella.[23,24] The WAXD signal at a value of q of 0.56, corresponding to α-helical secondary structures, remained almost unchanged upon

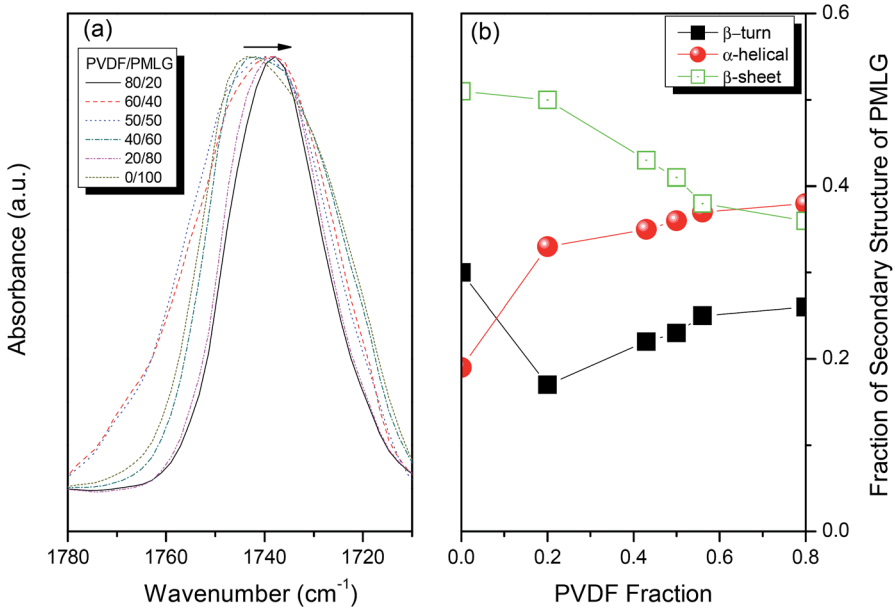

Fig. 3 (a) FTIR spectra (1780–1710 cm^{-1}, recorded at room temperature) and (b) secondary structures of the PVDF/PMLG blends.

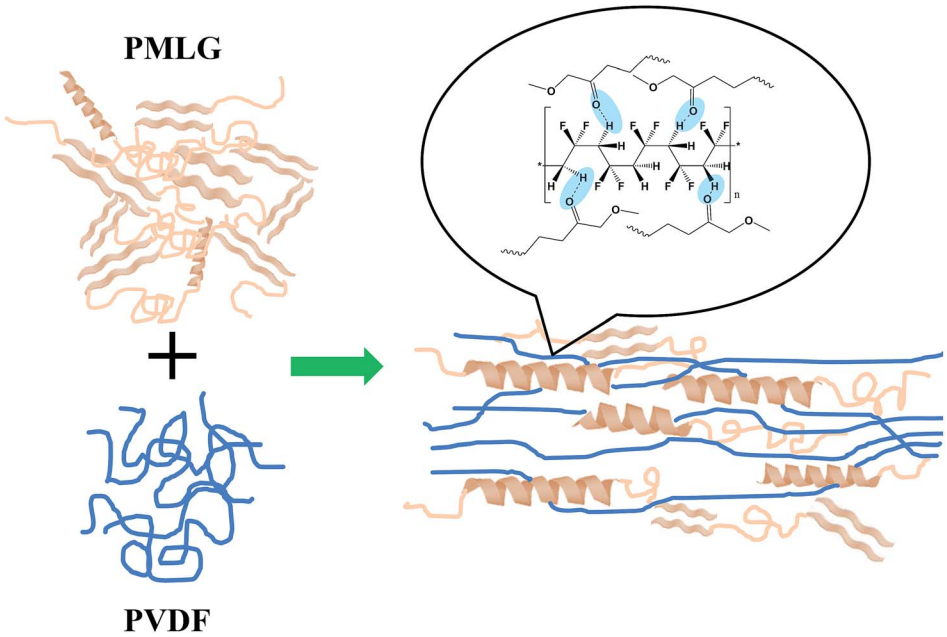

Scheme 2 Conformation changes and specific interactions between PVDF and PMLG fibers.

increasing the PVDF content; in contrast, the intensity of the signal at a value of q of 0.38, reflecting the β-pleated sheet structure, decreased accordingly. This result indicates that the α-helical conformation was stabilized, through intramolecular hydrogen bonding interactions, upon increasing the PVDF content, consistent with our conclusion from the FTIR spectroscopic analyses. In addition, pure PVDF provided WAXD diffraction peaks at values of q of 0.56, 1.41, 1.88, and 2.70 nm^{-1}, which can be indexed to, respectively, the α (020), β (110), α (021), and β (200) reflections of the crystalline PVDF conformation.[27–29] Upon increasing the content of PMLG, the intensity of the β peak decreased gradually, but the signal of the β-phase did not disappear completely until the PMLG content reached 80 wt%, similar to the behavior of the system in our FTIR spectroscopic analyses. Thus, to ensure a high fraction of α-helical secondary structures for PMLG and a high fraction of β-phase crystalline PVDF, we choose a blend composition of PMLG/PVDF = 60/40 for our subsequent experiments.

Characterization of PVDF/PMLG composite fibers after NFES processing

We used FTIR spectra to verify the structures of the PMLG/PVDF composite fibers after applying *in situ* electric poling and mechanical stretching effects of the NFES process. Fig. 5 displays the FTIR absorption spectra of the PMLG/PVDF powder and of the composite fibers prepared through NFES processing. After PMLG had been blended with PVDF, the fraction of β-sheets decreased and the fraction of α-helices increased, with better orientation, in both the powder and fiber forms, due to hydrogen bonding between the CH_2 group of PVDF and the C═O groups on the side chains of PMLG. The electric field appeared to have had a positive impact on the PVDF/PMLG piezoelectric characteristics of the α-helix. When we use NFES processing to fabricate the PVDF/PMLG composite fibers, the fraction of α-helical forms increased and the electric field resulted in both the PMLG and PVDF components becoming more orientated, as depicted in Scheme 2.

We employed a tensile test set-up [Fig. 6(a) and (b)] to investigate the ultimate stress and Young's modulus of the PVDF/PMLG composite fibers and to construct load–displacement curves to obtain critical information regarding their mechanical properties. Fig. 6(c)–(f) display the stress–strain curves of the PVDF/PMLG composite fibers under various electric fields (from 1×10^7 to 1.6×10^7 V m^{-1}). When we increased the applied electric field for the NFES process, the mechanical properties of the composite fibers improved, presumably because a higher electric field increased the stretching force, causing the fibers to become more compact and denser and strengthening the fibers' mechanical properties. Fig. 7 summarizes the relationship between the electric field and the Young's modulus and ultimate stress of the PVDF/PMLG composite fibers. When we prepared the PVDF/PMLG composite fibers under an electric field of 1.6×10^7 V m^{-1}, the ultimate stress was 27.47 MPa and the Young's modulus was 2.77 GPa. Thus, the ultimate stress of the PVDF/PMLG composite fibers was lower than that of the PVDF fibers, whereas the Young's modulus was greater. Because PMLG is a brittle material, PMLG/PVDF composite fibers would presumably be more brittle than pristine PVDF.

We designed a flexible piezoelectric harvester for operation under low-frequency ambient forces. Our fabrication of this harvester involved an *in situ* poling process; we controlled the dimensions of the piezoelectric fiber array by using a parallel electrode, allowing us to realize the conversion of mechanical to electrical signals. We employed a PET film to package the fiber arrays and to provide protection between the fibers and the

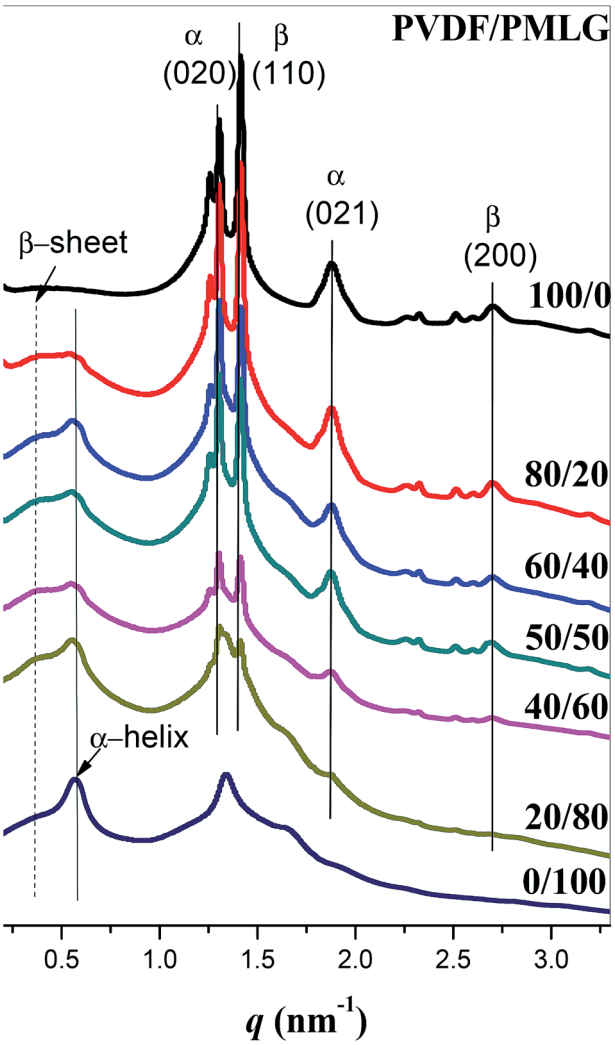

Fig. 4 Wide-angle X-ray diffractograms of PVDF/PMLG blends, measured at room temperature.

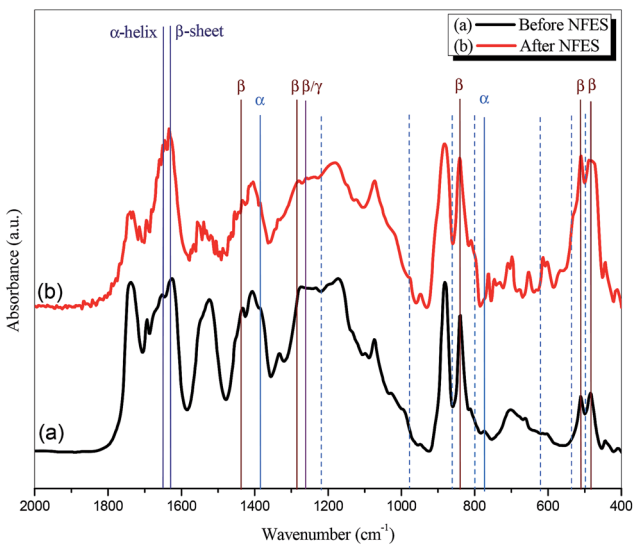

Fig. 5 FTIR spectra, recorded at room temperature, of PVDF/PMLG composite fibers (a) before and (b) after NFES processing.

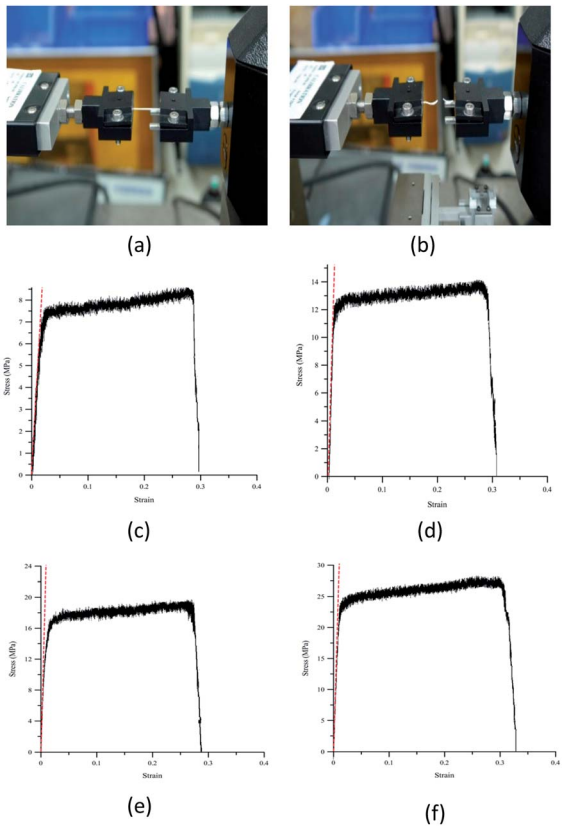

Fig. 6 (a and b) Schematic representation of the system (a) before and (b) after the tensile test and (c–f) stress–strain curves of PVDF/PMLG composite fibers prepared under electric fields of (c) 1×10^7, (d) 1.2×10^7, (e) 1.4×10^7, and (f) 1.6×10^7 V m^{-1}.

electrode, as well as prevent opposite charges from counteracting the electric potential. Fig. 8 displays the response of the induced electric potential upon applying a periodic force (a bending and releasing process) at 6 Hz. The peak voltage was approximately 0.113 V and the peak current was approximately 1.72×10^{-7} A for the PMLG/PVDF composite fibers at the strain rate of 0.03 s^{-1}. At the same strain rate, PMLG/PVDF composite fibers produced the largest voltage and current compared with pure PMLG and pure PVDF.

Next, we used tip deflection of the PET cantilever beam to measure the voltage, current, and strain from the flexible PMLG/PVDF harvesters under low-frequency vibrations (from 1 to 8 Hz). When we increased the frequency from 1 to 8 Hz, the force increased from 0.003 to 0.28 N, with a linear relationship between the voltage and the applied force, implying that such systems could be applied as force sensors (Fig. 9). It appears logical that a higher frequency would cause a larger strain rate that could then induce a higher voltage. Under vibrations of 1–8 Hz, the output voltages of the PVDF and PMLG fibers were 0.013–0.119 and 0.011–0.093 V, respectively, whereas those of the PMLG/PVDF composite fibers increased significantly to 0.019–0.185 V (Fig. 10). Thus, the presence of PMLG was effective at improving the piezoelectric properties of the PVDF/PMLG composite fibers.

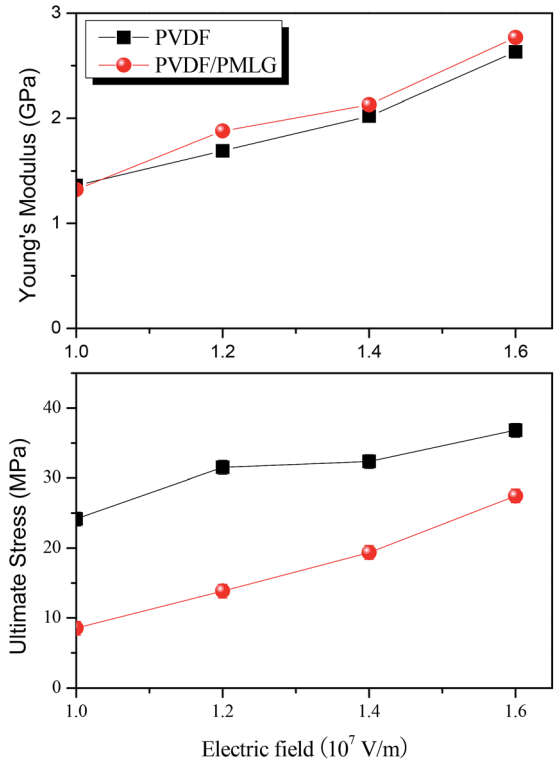

Fig. 7 Relationships between the electric field strength and the (a) Young's modulus and (b) ultimate stress of pure PVDF and PVDF/PMLG fibers.

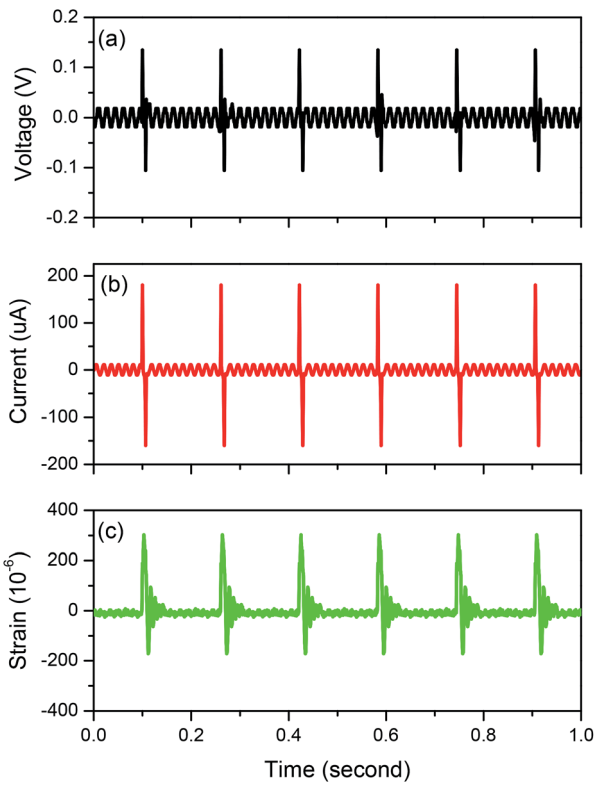

Fig. 8 (a) Voltage, (b) current, and (c) strain generated from the PMLG/PVDF fibers, measured under a vibration of 6 Hz.

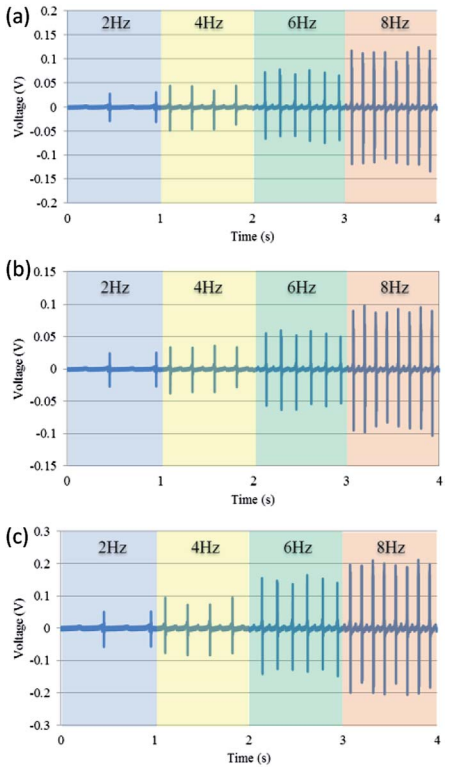

Fig. 9 Schematic representation of the frequency and voltage of (a) PVDF, (b) PMLG, and (c) PVDF/PMLG blends.

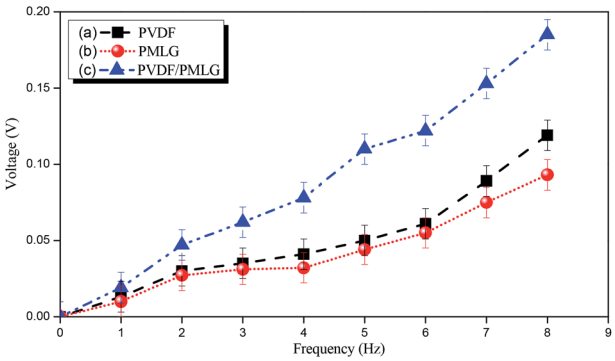

Fig. 10 Relationship between the frequency and voltage of (a) pure PVDF, (b) pure PMLG, and (c) PVDF/PMLG blends.

To obtain a better understanding of the powering outputs from the pristine PVDF, PMLG, and PVDF/PMLG composite harvesters, we fabricated fibers on a PET substrate with both ends tightly bonded to the Cu foil electrode pair, applying Ag paste at the ends of the fibers to fix the two ends tightly. A quick release of these electrons can induce a significantly large electric voltage/current pulse. Moreover, the PVDF, PMLG, and PVDF/PMLG harvesters could be modeled with a load resistor (RL) for the impedance matching test. Repeatedly stretching and releasing the harvester at a strain rate of 0.03 s^{-1} under a vibration of 6 Hz created a maximum peak voltage and power of 0.033 V and 293.107 pW, respectively, from the PVDF fibers with

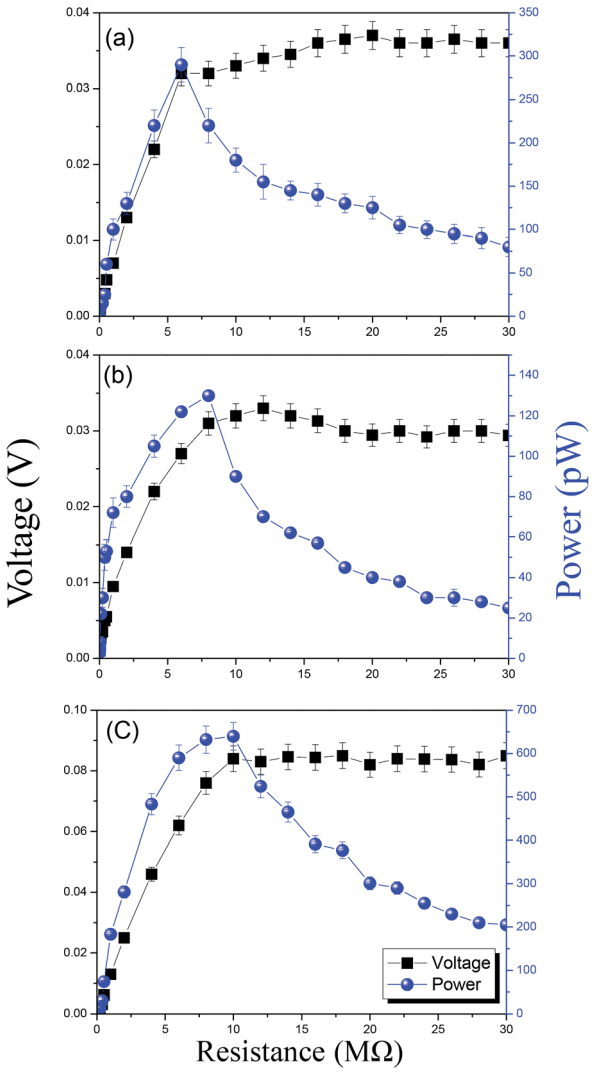

Fig. 11 Impedance matching tests of (a) pure PVDF, (b) pure PMLG, and (c) PVDF/PMLG blends.

an external load resistance of 6 MΩ; 0.033 V and 130.858 pW, respectively, from the PMLG fibers with an external load resistance of 8 MΩ; and 0.08 V and 637.81 pW, respectively, from the PMLG/PVDF composite fibers with a load resistance of 10 MΩ (Fig. 11). The theoretical maximum power is 19 435 pW based on the open circuit voltage = 0.113 V and closed circuit current = 172 nA and thus the energy conversion efficiency is 3.3% (637.81 pW/19 435 pW) in this study.

Conclusion

The NFES process has a positive impact on the piezoelectric and mechanical properties of PVDF/PMLG composite fibers, as a result of improving the orientation of the dipole and increasing the density. When tested at frequencies in the range from 1 to 8 Hz, the output voltages of the PMLG/PVDF composite energy harvester were 0.019–0.185 V, significantly higher than those of pure PVDF and pure PMLG. In addition, the electro-mechanical energy conversion efficiency of the energy harvester based on the PVDF/PMLG composite fibers is 3.3% which was up to three times higher than those of the corresponding devices based on pure PVDF and pure PMLG. This composite fiber displayed excellent piezoelectricity as a result of intermolecular hydrogen bonding between the PVDF and PMLG polymers and improved orientations of their rigid rods, suggesting that such systems might be applicable for use in sensors, actuators, biomedical engineering, and green energy.

Acknowledgements

This study was supported financially by the National Science Council, Taiwan, Republic of China, under contracts MOST103-2221-E-110-079-MY3 and MOST102-2221-E-110-008-MY3.

References

1 J. M. Tarascon and M. Armand, *Nature*, 2001, **414**, 359–367.
2 M. Armand and J. M. Tarascon, *Nature*, 2008, **451**, 652–657.
3 S. Fang, L. Shen, H. Zheng and X. Zhang, *J. Mater. Chem. A*, 2015, **3**, 1498–1503.
4 X. W. Gao, Y. F. Deng, D. Wexler, G. H. Chen, S. L. Chou, H. K. Liu, Z. C. Shi and J. Z. Wang, *J. Mater. Chem. A*, 2015, **3**, 404–411.
5 J. Fang, H. Niu, H. Wang, X. Wang and T. Lin, *Energy Environ. Sci.*, 2013, **6**, 2196–2202.
6 H. Zhang, Y. Yang, Y. Su, J. Chen, K. Adams, S. Lee, C. Hu and Z. L. Wang, *Adv. Funct. Mater.*, 2014, **24**, 1401–1407.
7 I. Iliuk, J. M. Balthazar, A. M. Tusset, J. L. P. Félix and B. R. D. Pontes, *Differ. Equ. Dyn. Syst.*, 2013, **21**, 93–104.
8 D. Sun, C. Chang, S. Li and L. Lin, *Nano Lett.*, 2006, **6**, 839–842.
9 C. Chang, K. Limkrailassiri and L. Lin, *Appl. Phys. Lett.*, 2008, **93**, 123111.
10 Z. H. Liu, C. T. Pan, L. W. Lin and H. W. Lai, *Sens. Actuators, A*, 2013, **193**, 13–24.
11 A. Greiner and J. H. Wendorff, *Angew. Chem., Int. Ed.*, 2007, **46**, 5670–5703.
12 Z. M. Huang, Y. Z. Zhang and K. S. Ramakrishna, *Compos. Sci. Technol.*, 2003, **63**, 2223–2253.
13 J. S. Andrew and D. R. Clarke, *Langmuir*, 2008, **24**, 670–672.
14 D. Farrar, K. Ren, D. Cheng, S. Kim, W. Moon, W. L. Wilson, J. E. West and S. M. Yu, *Adv. Mater.*, 2011, **23**, 3954–3958.
15 K. Ren, W. L. Wilson, J. E. West, Q. M. Zhang and S. M. Yu, *Appl. Phys. A*, 2012, **107**, 639–646.
16 C. T. Pan, C. K. Yen, L. Lin, Y. S. Lu, H. W. Li, J. C. C. Huang and S. W. Kuo, *RSC Adv.*, 2014, **4**, 21563–21570.
17 J. Hone, M. C. Llaguno, N. M. Nemes and A. T. Johnson, *Appl. Phys. Lett.*, 2000, **77**, 666.
18 H. S. Tzou, R. Ye and J. H. Ding, *J. Sound Vib.*, 2001, **241**, 271–281.
19 O. Breuer and U. Sundararaj, *Polym. Compos.*, 2004, **25**, 630.
20 C. T. Pan, C. K. Yen, Z. H. Liu and H. W. Li, *Sens. Mater.*, 2014, **26**, 63–73.
21 W. A. Yee, M. Kotaki, Y. Liu and X. Lu, *Polymer*, 2007, **48**, 512–521.

22 P. C. Painter, W. L. Tang, J. F. Graf, B. Thomson and M. M. Coleman, *Macromolecules*, 1991, **24**, 3929–3936.
23 P. Papadopoulos and G. Floudas, *Biomacromolecules*, 2004, **5**, 81–91.
24 S. W. Kuo and C. J. Chen, *Macromolecules*, 2011, **44**, 7315–7326.
25 S. W. Kuo and C. J. Chen, *Macromolecules*, 2012, **45**, 2442–2452.
26 S. W. Kuo, *J. Polym. Res.*, 2008, **15**, 459–486.
27 D. M. Dhevi, A. A. Prabu and M. Pathak, *Polymer*, 2014, **55**, 886–895.
28 J. W. Park, Y. A. Seo, I. Kim, C. S. Ha, K. Aimi and S. Ando, *Macromolecules*, 2004, **37**, 429–4369.
29 L. Yu and P. Cebe, *Polymer*, 2009, **50**, 2133–2141.
30 S. W. Kuo, W. J. Huang, C. F. Huang, S. C. Chan and F. C. Chang, *Macromolecules*, 2004, **37**, 4164–4173.
31 S. T. Li, Y. C. Lin, S. W. Kuo, W. T. Chuang and J. L. Hong, *Polym. Chem.*, 2012, **3**, 2393–2402.